Structure of the ion wakefield in dusty plasmas

G. A. Hebner and M. E. Riley
Sandia National Laboratories, Albuquerque, New Mexico 87185-1423, USA
(Received 8 September 2003; published 23 February 2004)

The magnitude and structure of the ion wakefield potential below a single negatively charged dust particle levitated in the plasma sheath region were measured using a test particle. Attractive and repulsive components of the interaction force were extracted from a trajectory analysis of low-energy collisions between different mass particles in a well-defined electrostatic potential that constrained the dynamics of the collisions to one dimension. As the vertical spacing between the particles increased, the peak attractive force decreased and the width of the potential increased. For the largest vertical separations measured in this study, the lower particle does not form a vertical pair with the upper particle but rather has an equilibrium position offset from the bottom of the parabolic potential confining well.

DOI: 10.1103/PhysRevE.69.026405 PACS number(s): 52.27.Lw, 52.27.Gr, 52.30.−q, 52.20.−j

I. INTRODUCTION

The addition of dust to a plasma leads to a number of long range and collective interactions that influence the characteristics of interstellar regions, planetary rings, fusion reactors, and laboratory microelectronics processing systems. Particle-particle interactions and the forces that drive the interactions depend on a myriad of variables such as plasma characteristics, dust density and material, external potentials, and the flow of charged species past the particles. For example, ion flow around the particles generates an ion wind force on the particles due to momentum transfer. In addition, positive ion flow around the negatively charged particles warps the sheath structure around the particle and generates a wakefield or a net positive space charge region downstream from the particle due to ion focusing [1–4]. The positive space-charge region gives rise to an attractive interaction between the negatively charged particles and is the origin of a number of collective interactions in dusty plasmas.

It is well known that dust particles levitated at the plasma sheath can form single-layer [two-dimensional (2D)] hexagonal-close-packed, triangular lattice structures that are dominated by repulsive screened Coulomb (Debye) interactions [5–8]. Multilayer 3D assemblies in dusty plasmas show a range of order from face- and body-centered cubic lattices to more amorphous arrangements [9–12]. In the simplest view, the lattice arrangement of multilayer structures appears to depend on the delicate balance between an attractive ion wakefield potential and repulsive Debye potentials [9,13]. However, this simple view is not universally accepted because the largest 3D dust arrangements apparently show little wakefield effect [14]. Thus the full impact of the attractive interaction on dusty plasma collective interactions appears to be an open question.

Several recent measurements have begun to address this issue. Melzer and co-workers observed a nonreciprocal attractive interaction between two different mass particles [15,16]. We recently measured peak attractive interactions in 60 and 100 mTorr argon plasmas that were on the order of 200 fN [17,18]. Our technique determined the shape of the entire attractive and repulsive potential from an analysis of constrained 1D collisions between particles that originate at far distances from each other. We found that the peak attractive potential increased with lower pressure, likely due to an increased ion mean free path. In addition, the attractive potential had a finite vertical extent that decayed fairly rapidly with vertical particle separation.

The structure of the ion wakefield has been calculated by several groups, each using various simplifying assumptions for this computationally challenging problem [1,4,17,19,20]. The calculations show the formation of a positive space charge region downstream of the particles and a warping of the symmetric sheath that would be expected in the absence of the streaming ions present at the sheath boundary. The extent of the positive space charge region is on the order of the Debye screening length, 50–400 μm for our experimental conditions. Under certain conditions, the resulting positive space charge region can produce relatively strong attractive electrostatic interactions with other particles. However, we note that even the basic idea of electrostatic attraction is open to discussion [21].

This paper expands on our previous work to measure the planar attractive and repulsive interaction potentials associated with a single dust particle levitated at the plasma sheath edge as a function of the vertical position. The result is a full 3D measurement of the particle force field. In most terrestrial dusty plasma systems, the ion wakefield dimensions are on the order of the plasma Debye length (50–500 μm) and usual probe techniques are not possible. By using a constant particle diameter for the upper particle and a range of particle diameters for the lower particle, and thus a range of vertical separations, we can map the shape of the attractive ion wakefield potential from an analysis of the particle collision dynamics. As the vertical spacing between the particles was increased, we observed a transition from repulsive, nonvertically aligned pairs, to attractive vertically aligned pairs, and then back to nonvertically aligned pairs. The first nonpaired to paired transition has been previously observed and measured [13,16,18,22]. However, the second aligned to unaligned transition was unexpected and indicates that the 3D structure of dusty plasma assemblies depends critically on the dust characteristics and plasma conditions.

II. EXPERIMENTAL SETUP

The experiments were performed in an asymmetrically driven, parallel-plate discharge chamber, a modified Gaseous Electronics Conference (GEC) rf reference cell [23]. The details of this chamber and experimental technique have been previously reported so only a brief overview is presented [17]. The lower electrode was capacitively coupled and driven at 20 MHz and 0.9 W. Argon gas flow was 2 sccm at 100 mTorr. The 10 cm diameter lower electrode contained a 5 cm diameter insert that was machined with a 0.5 m radius of curvature spherical shape [5,17]. Following the slight curvature, we machined a slot 3 mm wide and 2 mm deep across the diameter of the insert. The electrode slot forms a steep potential gradient (''electrostatic trench'') perpendicular to the line defined by the slot, with a curvature that is on the order of the plasma sheath thickness, approximately 5 mm [18]. With this arrangement we could reproducibly generate collinear collisions with a constant vertical offset (impact parameter) using two particles of different mass. The vertical confining forces (electric sheath, gravity, and ion wind) are much stronger than the weak particle-particle interactions or random Brownian motion, resulting in collision dynamics constrained to motion in the coordinate axis parallel to the trough. The vertical movement of the injected particles damped quickly, as did any oscillation normal to the trough. In addition, the amplitude of Brownian motion normal to the trough was considerably less than the particle's distance of closest approach.

The particles were illuminated by a sheet of light produced by a 532 nm, 10 mW laser, scanning mirror and cylindrical lens. Top and side views of the time-dependent particle trajectories were captured on videotape using two CCD cameras and lenses. The videotape was digitized frame by frame and the particle position extracted using image analysis algorithms. The time spacing was 30 frames/sec and the pixel resolution for this work was 0.035 mm/pixel.

The electrostatic trench was used for two different measurements. The first used particles of the same mass, and hence the same height above the lower electrode, to determine the particle charge Z and plasma screening length λ from an analysis of the radially dependent particle spacing resulting from gravitational compression. Since that analysis has been previously discussed, only the results for the particle Z and λ are presented in this paper [18]. For these experimental conditions, particle charge and screening length increased linearly from 6000 to 18 000 electrons, and 300 to 600 μm for particle diameters from 6.86 to 11.93 μm, respectively. These values are consistent with our previous measurements [17,18].

The second set of experiments, and the focus of this work, was measurement of the wakefield potential associated with an upper target dust particle obtained by colliding it with a probe dust particle levitated at a lower height. For these measurements, a single Melamine particle was dropped into one end of the trough and fell to the bottom of the spherical electrode with a damping time constant determined by gas drag [5]. At a later time, a second particle with a different diameter, hence a different height above the lower electrode, was dropped into the opposite end of the trough. The particle collision dynamics were recorded on videotape. Time-dependent particle positions were extracted from the digitized videotape and analyzed for the interaction force.

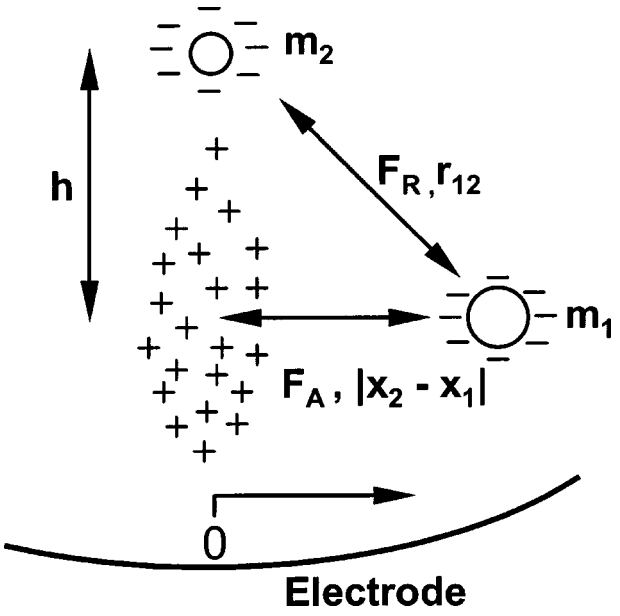

FIG. 1. Schematic of two particles showing upper particle of mass m_2, lower particle of mass m_1, and ion wakefield (positive space charge region) below the upper particle. The 0.5 m radius of curvature of the lower electrode is greatly exaggerated. The height difference between the particles was h and the interparticle separation was r_{12}. The center of the well is defined as zero and the horizontal distance of the particles from the center of the well is x_1 or x_2.

III. WAKEFIELD POTENTIAL STRUCTURE

A schematic of the simplified particle interaction is shown in Fig. 1. The upper particle of mass m_2 has a smaller diameter and mass than the lower particle of mass m_1. Considering only dominant interactions, the upper particle interacts with the lower particle via repulsive interactions arising from the screened Coulomb potentials as characterized by each particle's Z and some λ appropriate for the pair. However, the lower particle also reacts to an electrostatic attractive interaction between the positive space charge region and the negative dust particle's surface charge, in addition to the reciprocal repulsive interactions with the upper particle. While there is also a space charge region below the lower particle, for our conditions, we estimate that it does not strongly interact with the negative charge of the upper particle due its relatively large distance and thus we do not include it in our force analysis. Only the horizontal distance between the particles is shown or analyzed. The vertical distance between the particles varied by less than 0.02 mm, reflecting the strong vertical confining forces and the lack of changes in the particle charge.

The interaction potentials are obtained from the particles' position and velocity by numerically inverting the (Newtonian equations of motion) (NEOM) shown below. Due to the

experimental geometry and vertically constrained motion, we have only a 1D set of equations. The upper particle interacts with the lower particle through a repulsive potential $V_D(r_{12})$ where $r_{12}=\sqrt{(x_1-x_2)^2+h^2}$, with h the vertical spacing between the particles, and x_i the Cartesian coordinate parallel to the trough (Fig. 1). The lower particle, however, responds to both the above repulsive interaction and an attractive force generated between it and the wakefield $V_A(|x_1-x_2|,h)$. In this limit, the NEOM for the two particles are

$$m_1\ddot{x}_1+m_1\gamma_1\dot{x}_1+k_1x_1=\left(\frac{x_2-x_1}{r_{12}}V_D'-\frac{\partial}{\partial x_1}V_A(|x_1-x_2|,h)\right), \tag{1}$$

$$m_2\ddot{x}_2+m_2\gamma_2\dot{x}_2+k_2x_2=\frac{x_1-x_2}{r_{12}}V_D'(r_{12}), \tag{2}$$

where m_i is the mass, γ_i is the Epstein drag coefficient, and $k_i=m_ig/R_c$ with g the acceleration due to gravity and R_c the radius of curvature of the electrode. The subscript 1 denotes the lower particle and the subscript 2 denotes the upper particle. Solving for the attractive force $f_A=-(\partial/\partial x_1)V_A(|x_1-x_2|,h)$ and the repulsive force $f_R=V_D'(r_{12})$ as functions of the interparticle spacing yields

$$f_A=m_1\ddot{x}_1+m_1\gamma_1\dot{x}_1+k_1x_1+m_2\ddot{x}_2+m_2\gamma_2\dot{x}_2+k_2x_2, \tag{3}$$

$$f_R=\frac{r_{12}}{x_1-x_2}[m_2\ddot{x}_2+m_2\gamma_2\dot{x}_2+k_2x_2]. \tag{4}$$

Thus the attractive and repulsive potentials can be derived from only the particle positions as functions of time. The first and second derivatives (velocity and acceleration) were calculated after three-point smoothing was performed on the time-dependent position data. Experimentally measured Epstein gas-damping rates (100mTorr) of 27, 21, 17, 15, 14, 14, and 12 s^{-1} were used for the 6.86, 8.89, 9.78, 10.45, 11.55, 11.93, and 12.74 μm diameter particles, respectively. Rather than use calculated Epstein drag coefficients, we experimentally determine the values for each experimental condition, since we find that the value of the attractive force, which should be zero for large particle separations, depended strongly on the value of the gas drag. As in previous work, the measured drag coefficients are in good agreement with calculated values to within the uncertainty introduced by the dominant neutral scattering mechanism and gas temperature [6,24]. As the lower particle moves into the space charge region, it will change the shape of the ion wakefield potential. Because we know the confining force due to the curved electrode, the drag force due to neutral gas scattering, and the charges of the particles by single-layer analysis [5,6], we can isolate the *full* interaction of the particles. The ion wakefield potential can be obtained by integrating the force maps.

Experimentally determined attractive forces are shown in Fig. 2 as functions of the horizontal particle separation $|x_2-x_1|$, and vertical particle spacing. Data from four to eight collision events is shown within each plot. Whether an upper particle was injected towards the already present lower particle or visa versa made no difference, as previously observed. For these experimental conditions, the peak attractive force decreased from 70 to 10 fN as the vertical particle separation increased from 0.56 to 1.16 mm (graphs a–d). The width of the attractive force also increased by a factor of two over this range of particle separations. The maximum force was obtained at horizontal particle separations between 200 and 300 μm. Thus the ion wakefield potential has a finite vertical extent and decays fairly rapidly with vertical distance below the upper particle. These observations are consistent with most models of the wakefield potential [1,4,17,19,20].

Experimentally determined repulsive force maps are shown in Fig. 3 as functions of the absolute particle separation r_{12} and vertical particle spacing. Due to the (x_2-x_1) term in the denominator of Eq. (4), the repulsive data became noisy as the particles formed a vertical pair and is not shown. For these experimental conditions, the repulsive force decreased from 30 to 7 fN as the vertical particle separation increased from 0.56 mm to 1.16 mm (graphs a–d). The shape and magnitude of the repulsive interaction was similar for these four sets of particles, only the maximum distance between the particles varied. Thus it appears that the repulsive force is dominated by the upper particle, whose characteristics do not change. This is somewhat surprising since the lower particle charge and screening length increase with diameter and one would think that the repulsive force should increase proportionally. This may indicate that as the lower particle enters the space charge region, the shielding of the space-charge cloud modifies the electrostatic repulsion. It is unlikely that the particle charge changes significantly since the vertical height of the lower particle, determined by the time-average electric field and particle charge, does not change.

The solid lines shown in Figs. 2 and 3 are regression fits to functional forms for the attractive and repulsive potential. The repulsive force was fit to a screened Coulomb form $[V_D(r_{12})=(Z^2/4\pi\varepsilon_0)\exp(-r_{12}/\lambda)/r]$. Previously we showed that the dominant cylindrical radial dependence of the wakefield potential was

$$V(r)=A_W\exp(-\sqrt{a^2+r^2}/\lambda), \tag{5}$$

where A_W is a function of plasma and dust parameters, and a depends on the thermal averaging of ion motion [17]. In general, the fits for both the attractive and repulsive potentials are good. Values for the attractive and repulsive fit parameters are shown in Tables I and II. The fit to the repulsive force yields and A_W value that is consistent with our measured particle charge but a λ that is approximately a factor of 2 larger than that derived from an analysis of the particle monolayer compression [6]. The larger value of the screening length is approaching the electron Debye length. We hypothesize that this is due to the higher ion velocity in the vicinity of the particles, giving less ion screening and a larger Debye length. However, the use of a single screening length to describe the repulsive interaction between two particles with unequal screening lengths is not physical and needs to be modified.

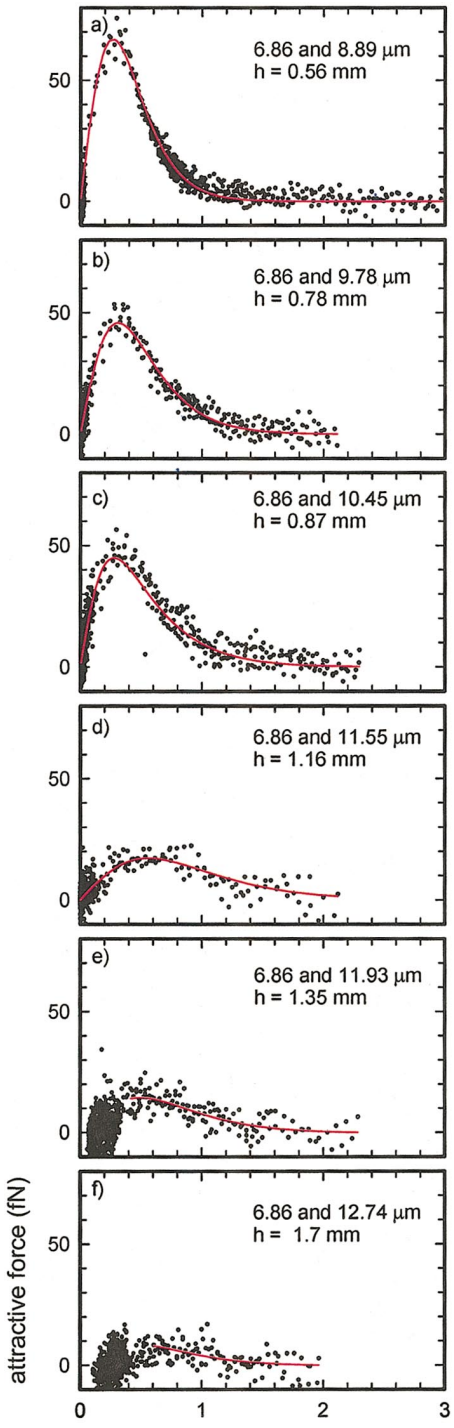

FIG. 2. (Color) Ion wakefield attractive forces as functions of the horizontal interparticle spacing and vertical spacing. The particle diameter are shown in each plot. The data points are shown as points while the lines are fits to the attractive potential form described by Eq. (5). The fit parameters are in Table I.

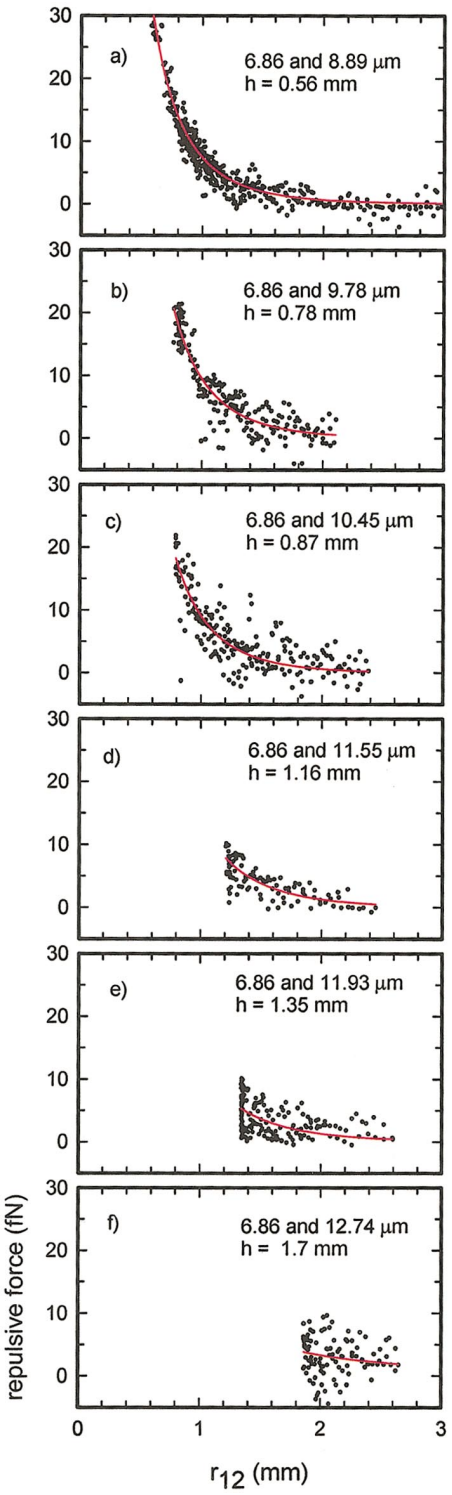

FIG. 3. (Color) Ion wakefield repulsive potentials as functions of the interparticle spacing and vertical separation. The particle diameters are shown in each figure. The data points are shown as points while the lines are fits to a screened Coulomb potential of the form $V_D(r_{12})=(Z^2/4\pi\varepsilon_0)\exp(-r_{12}/\lambda)/r$. Fit parameters are in Table II.

The shape of the potential associated with each attractive interaction can be obtained by either integrating the data or from fit parameters and Eq. (5). The potentials determined from the fits to the data in Figs. 2(a)–2(d) are shown in Fig. 4. In each case, the interaction is assumed to be electrostatic and the different particle charges are divided out of the calculation of the potential. The peak potential well depth decreased from 21 to 8 mV as the distance below the upper test particle increased from 0.56 to 1.16 mm. The width of the potential well also increased. It should be noted that the

TABLE I. Values for regression fits to the attractive potential given by Eq. (5) for various lower particle diameters. The upper particle diameter was 6.86 μm.

Diameter (μm)	A_W/λ (10^{-14} N)	λ (μm)	a (μm)
8.89	−380	167	485
9.78	−83	244	470
10.45	−24	331	312
11.55	−36	430	873
11.93	−68	316	864
12.74	−139	254	975

variation of the potential well due to the ion wakefield in the *radial* direction is superimposed on the much larger potential variation in the *vertical* direction due to the sheath structure. For example, for a particle charge of 6000 electrons, the 6.86 μm particle requires a time-average electric field on the order of 30 V/cm to levitate. Over the 0.56 to 1.16 mm difference in heights measured here, this corresponds to a vertical potential variation of 1800 mV.

In contrast to the vertically aligned pairs analyzed above, particles with the largest vertical separations of 1.35 and 1.7 mm (graphs e and f in Figs. 2 and 3) form nonvertically aligned pairs. As shown in Fig. 5, when the lower particle collided with the upper particle, the two particles do not vertically pair but form an offset pair. In addition, the details of the offset pair structure appear to also depend on vertical spacing. In the case of the 11.93 μm diameter particles with a vertical separation of 1.35 mm from the 6.86 μm diameter particle, the lower particle pushed the upper particle away from the center of the parabolic confining potential. The minimum energy state appears to have the two particles splitting the difference in the potential energy obtained by the particles not being at the bottom of the well ($r=0$ mm). However, in the case of the 12.74 μm diameter particle with a vertical spacing of 1.7 mm, the lower particle lacks the force required to move the upper particle significantly away from the center of the potential well. In this case, the lower particle assumes all the potential energy by sitting offset from the bottom of the well. The nonaligned pairs were not due to gas flow or experimental asymmetries since the final location of the lower particle with respect to the upper particle depended on which side of the trench the lower particle was added. Side views of the videotaped collisions show that

TABLE II. Values for regression fit to the repulsive potential given by a screened Coulomb functional form for various lower particle diameters. The upper particle diameter was 6.86 μm.

Diameter (μm)	A (10^{-20} J m)	λ (μm)
8.89	1.4	630
9.78	2.0	576
10.45	2.0	556
11.55	2.5	675
11.93	2.1	744
12.74	1.3	3840

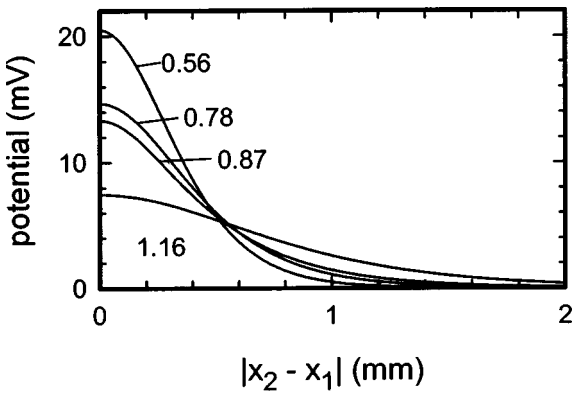

FIG. 4. Potential wells determined from the fits to the attractive potentials shown in Fig. 2. The numbers are the distance below (downstream) the upper 6.86 μm diameter particle.

lower particles added to the left side of the upper particle always stayed on the left and lower particles added on the right always stayed on the right.

The data in Figs. 2(e) and 2(f) were fit to the attractive potential over a limited range. Since the pairs do not form a vertically aligned pair, the fit is not appropriate for the region close to $|x_2-x_1|=0$. However, this functional form does appear to be appropriate over a limited range, at least up to the point were their attractive force is counterbalanced by a stronger repulsive force.

There are a number of possible origins for the force responsible for the nonvertically aligned pairs at the largest interparticle spacing. For example, the nonvertically aligned

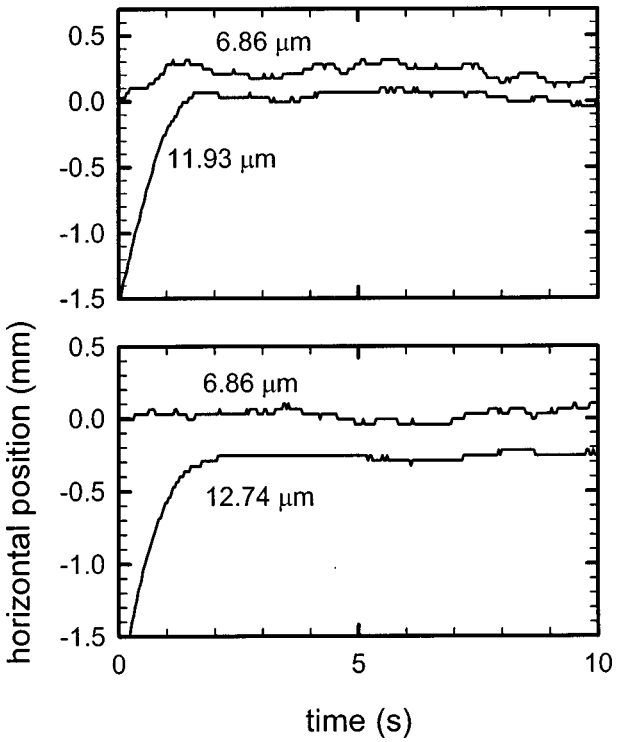

FIG. 5. Time-dependent horizontal positions of the nonvertically aligned particles after the addition of the lower particle. Particle diameters are shown in the plots.

orientation of the particles could be due to the influence of a nonperpendicular ion wind. For the largest vertical spacing, the ion wind is no longer perpendicular to the electrodes but has been focused by the upper particle. As the particle separation increases, the attractive potential clearly decreases until at some point it becomes less than the horizontal component of the ion wind. Arguing against the ion wind is the radially symmetric nature of the ion wind force. Ion charge-exchange collisions leading to fast neutrals are also a possibility. Collisions between the focused ion wind and the background gas will give rise to fast neutrals with a vector direction that tends to point away for the center of the well. Subsequent collisions with the neutral particle would provide an outward directed force. These suggested mechanisms are clearly working arguments that must be tested in future experiments.

IV. SUMMARY

The magnitude and structure of the attractive ion wakefield potential below a negatively charged dust particle levitated in the plasma sheath region was measured as a function of the interparticle spacing. The ion wakefield force field generated by an upper lighter target dust particle was determined by colliding it with a heavier probe dust particle levitated at a lower height. Attractive and repulsive interactions between charged particles were calculated using Newton's equations for a number of experimental conditions. This method does not assume a form for the interaction potential. For these conditions, the peak attraction was 70 fN and decreased with increasing vertical separation. The width of the attractive interaction increased with increasing vertical separation. Fits to the attractive force are in good agreement with our derived functional form while the repulsive forces are in good agreement with the classic screened Coulomb potential.

As the vertical spacing between the particles was increased, we observed a transition from repulsive, nonvertically aligned pairs, to attractive vertically aligned pairs, and then back to nonvertically aligned pairs. For the largest vertical separations measured in this study, the lower particle did not form a vertical pair with the upper particle but rather had an equilibrium position offset from the bottom of the parabolic potential confining well. We hypothesize that the nonvertically aligned orientation of the particles is due to the influence of fast neutral collisions. However, future experiments and models will be required to verify this proposal. While caution must be observed in extrapolating one limited set of measurements, our observation that the vertical alignment of the particle pairs depends on the interparticle spacing partially explains the wide variety of particle arrangements that have been previously observed in multiplayer particle assemblies.

ACKNOWLEDGMENTS

This work was supported by the Division of Material Sciences, BES, Office of Science, U.S. Department of Energy and Sandia National Laboratories, a multiprogram laboratory operated by Sandia Corporation, a Lockheed Martin Company for the United States Department of Energy's National Nuclear Security Administration under Contract No. DE-AC04-94AL85000.

[1] V. A. Schweigert *et al.*, Phys. Rev. E **54**, 4155 (1996).
[2] A. Melzer, V. A. Schweigert, I. V. Schweigert, A. Homann, S. Peters, and A. Piel, Phys. Rev. E **54**, R46 (1996).
[3] V. N. Tsytovich, Phys. Usp. **40**, 53 (1997).
[4] M. Lampe *et al.*, Phys. Plasmas **7**, 3851 (2000).
[5] G. A. Hebner *et al.*, Phys. Rev. Lett. **87**, 2350011 (2001).
[6] G. A. Hebner, M. E. Riley, and K. E. Greenberg, Phys. Rev. E **66**, 046407 (2002).
[7] G. A. Hebner *et al.*, IEEE Trans. Plasma Sci. **30**, 94 (2002).
[8] U. Konopka, G. E. Morfill, and L. Ratke, Phys. Rev. Lett. **84**, 891 (2000).
[9] K. Takahashi *et al.*, Phys. Rev. E **58**, 7805 (1998).
[10] J. B. Pieper, J. Goree, and R. A. Quinn, Phys. Rev. E **54**, 5636 (1996).
[11] Y. Hayashi, Phys. Rev. Lett. **83**, 4764 (1999).
[12] G. E. Morfill *et al.*, Phys. Rev. Lett. **83**, 1598 (1999).
[13] V. Steinberg *et al.*, Phys. Rev. Lett. **86**, 4540 (2001).
[14] M. Zuzic *et al.*, Phys. Rev. Lett. **85**, 4064 (2000).
[15] A. Melzer, V. A. Schweigert, and A. Piel, Phys. Rev. Lett. **83**, 3194 (1999).
[16] A. Melzer, V. A. Schweigert, and A. Piel, Phys. Scr. **61**, 494 (2000).
[17] G. A. Hebner, M. E. Riley, and B. M. Marder, Phys. Rev. E **68**, 016403 (2003).
[18] G. A. Hebner and M. E. Riley, Phys. Rev. E **68**, 046401 (2003).
[19] S. V. Vladimirov, S. A. Maiorov, and N. F. Cramer, Phys. Rev. E **67**, 016407 (2003).
[20] F. Melandso and J. Goree, Phys. Rev. E **52**, 5312 (1995).
[21] G. Lapenta, Phys. Rev. E **66**, 026409 (2002).
[22] S. V. Vladimirov and A. A. Samarian, Phys. Rev. E **65**, 046416 (2002).
[23] P. J. Hargis, Jr. *et al.*, Rev. Sci. Instrum. **65**, 140 (1994).
[24] P. S. Epstein, Phys. Rev. (Series 2) **23**, 710 (1924).